Numerical modeling of the effect of variable wind direction on migration of sand dunes at Jockey's Ridge, North Carolina

Victoria Thompson

Charlottesville, Virginia

A Thesis presented to the Undergraduate Academic Review Committee of the University of Virginia in Candidacy for the Bachelor of Science Distinguished Major Degree

Department of Environmental Sciences

University of Virginia

May 2024

Supervising Faculty:

Ajay Limaye

Abstract

Jockey's Ridge State Park in the Outer Banks of North Carolina hosts the largest sand dunes in the eastern US. These dunes are migrating southward, causing massive quantities of sand to threaten nearby infrastructure including houses and roads. Numerical models could help improve forecasts for dune migration and have been previously applied to Jockey's Ridge assuming a unidirectional wind field. However, a major knowledge gap remains for predicting dune migration under seasonal winds that vary in magnitude and direction. To address this gap, I rebuilt a reduced-complexity model for sand dune development (Werner, 1995; Pelletier et al., 2009) and extended the model to account for winds in any direction. I found that in model scenarios seeded with random initial topography, bimodal wind directions favor (1) the formation of dunes as connected ridges instead of isolated, crescentic barchans dunes; and (2) slower dune migration. I then ran a hindcast for Jockey's Ridge from 1999 to 2008 to compare model predictions with and without variable wind directions to observed migration patterns. These comparisons show that the model with variable wind directions predicts more westerly migration and taller dunes compared to observed topographic evolution and predictions from existing models. This work establishes a foundation for future efforts to relate dune migration to wind fields at Jockey's Ridge and provides actionable predictions for managing dune migration in the coming decades.

Acknowledgements

To my advisor, Professor Ajay Limaye, without whom this thesis would not have been possible. Thank you for always being my biggest advocate and for allowing me to weasel my way into the Landscape Evolution Group my third year. From trusting me to work in your mountaintop lab to hosting four-hour coding meetings before dawn, your selflessness knows no bounds. I truly will never be able to thank you enough for all you have done to support my academic and professional career.

To Youwei Wang and the other members of the Landscape Evolution Group, thank you all for believing in me as a resarcher and providing such valuable time and input into my project.

To my parents and sister, thank you for your unwavering support in my career in environmental science. I am eternally grateful to have a family who make my dreams come true and whose support gets me through the tough research days.

To my grandfather, Richard Fremon, whose interest in my project drove me to make it the best it could be. Thank you for inspiring my love of science from such a young age.

To Caroline Parmentier, thank you for making those early mornings and late nights in the GIS lab a lot less lonely.

—

This project is dedicated my grandmother, Rosalie Thompson, who passed during the completion of this this thesis. She inspired my love of the natural world and is the reason why I am where I am today.

Table of Contents

List of Figures

List of Tables

1 Introduction

1.1 Dunes and dune migration

Predictive modeling of landscape evolution is based on known physical processes and properties (Marín et al., 2005). Aeolian landscapes with sand dunes have been the targets of such modeling for several decades (e.g. Werner, 1995; Pelletier et al., 2009; Swanson et al., 2017). A dune is a mound of sand consisting of several key physical attributes formed by wind (Figure 1).

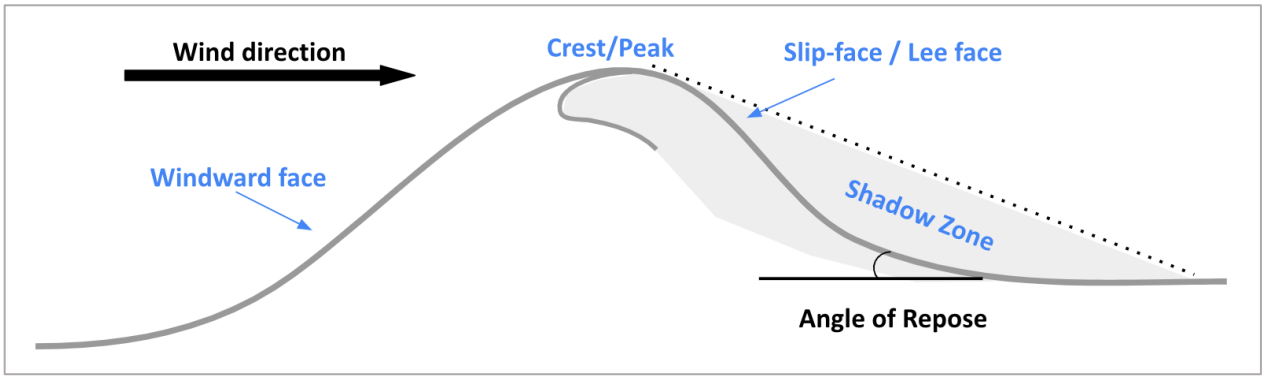

Figure 1. Side profile of a dune labeled with its key physical components. Wind flows over the dune onto the windward face. Sand reaches the crest, then rolls down the slip-face into the wind shadow. Wind cannot reach the sand in the shadow zone. All dunes, regardless of shape, have these same components.

Like many other landforms, aeolian dunes evolve through feedback between wind flow, sediment transport, and topography (Gadal et al., 2022). Dune fields, which contain multiple dunes in proximity, are semi-arid landscapes formed in a process driven by wind and precipitation (Tsoar, 2005). Dunefields are active landscapes that constantly evolve ecologically and physically (Jefferys et al., 2019).

The shape and behavior of dunes is significantly impacted by wind direction and variability (Paris et al., 2019). Specifically, the shape of an individual dune is determined by the relationship between the wind direction and the sand supply (Figure 2). Transverse dunes and

barchans are formed from unimodal winds (i.e. wind blowing from one primary direction) while other dune types are formed from winds blowing in multiple directions (Paris et al., 2019). Barchans are one of the most common dune types, and they consist of a body and horns (Hersen, 2004). When they combine with other parallel barchans, they form barchanoid ridges.

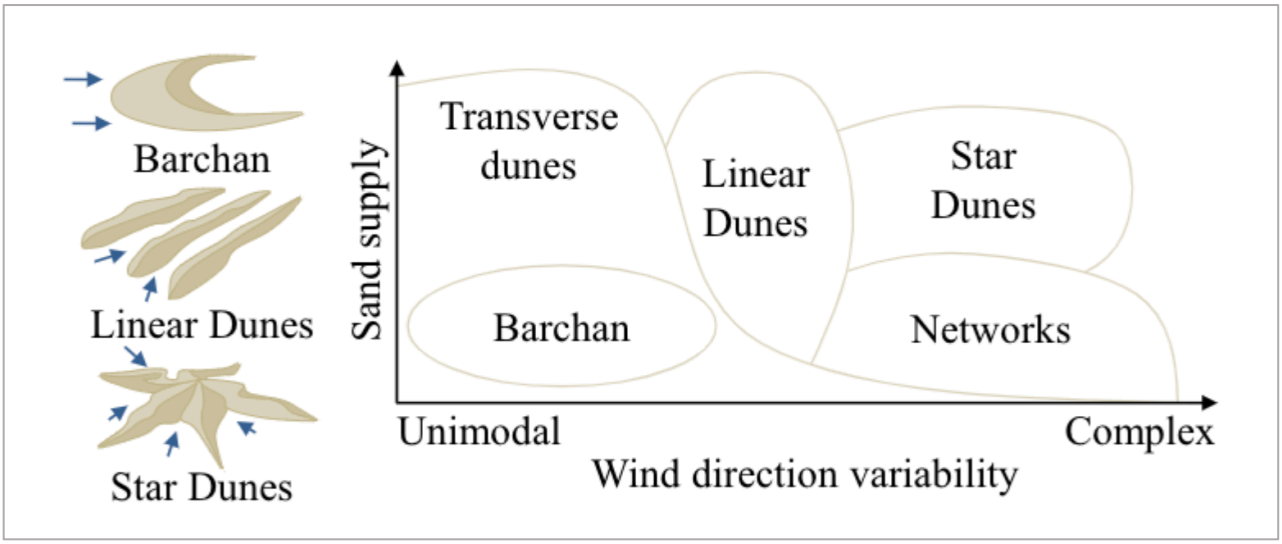

Figure 2. The relationship between wind direction variability and sand supply. Unimodal winds with low sand supply lead to the formation of barchans. As sand supply increases, these dunes become more transverse-shaped. Linear dunes are formed with the same sand supply, but with bi-directional winds. This figure is adapted from (Paris et al., 2019), their Figure 2.

Along with dune shape, dune motion is also affected by wind variability (Marín et al., 2005). There are three primary modes of aeolian dune movement. A dune is considered migrating if the whole dune body advances with minimal change in dimension and shape (Tsoar et al., 2004). An elongating dune changes length, and an accumulating dune changes volume (Tsoar et al., 2004). Wind direction is crucial in determining which process a dune undergoes. The difference between these three dune motion types (migrating, elongating, and accumulating) is caused by the index of directional wind variability, which is calculated as

$$DV = RDP/DP \quad (1)$$

If wind generally comes from one direction, the index approaches 1; if wind is multidirectional, the index approaches 0 (McKee, 1979). In most cases where dune migration is unidirectional, RDP/DP ≥ 0.8; however, in numerical models, the ratio is often set to the idealized value of 1. Dune migration leads to overall displacement if the DV is high. Therefore, the directionality of wind is a critical control of dune formation and migration and must be accounted for to generate robust predictions from numerical models.

1.2 Case study: Jockey's Ridge, NC

Beyond its role in landscape evolution, dune migration can have major consequences for manufactured infrastructures. A pertinent example occurs at Jockey's Ridge State Park, located on a barrier island in the Outer Banks of North Carolina (Figure 3).

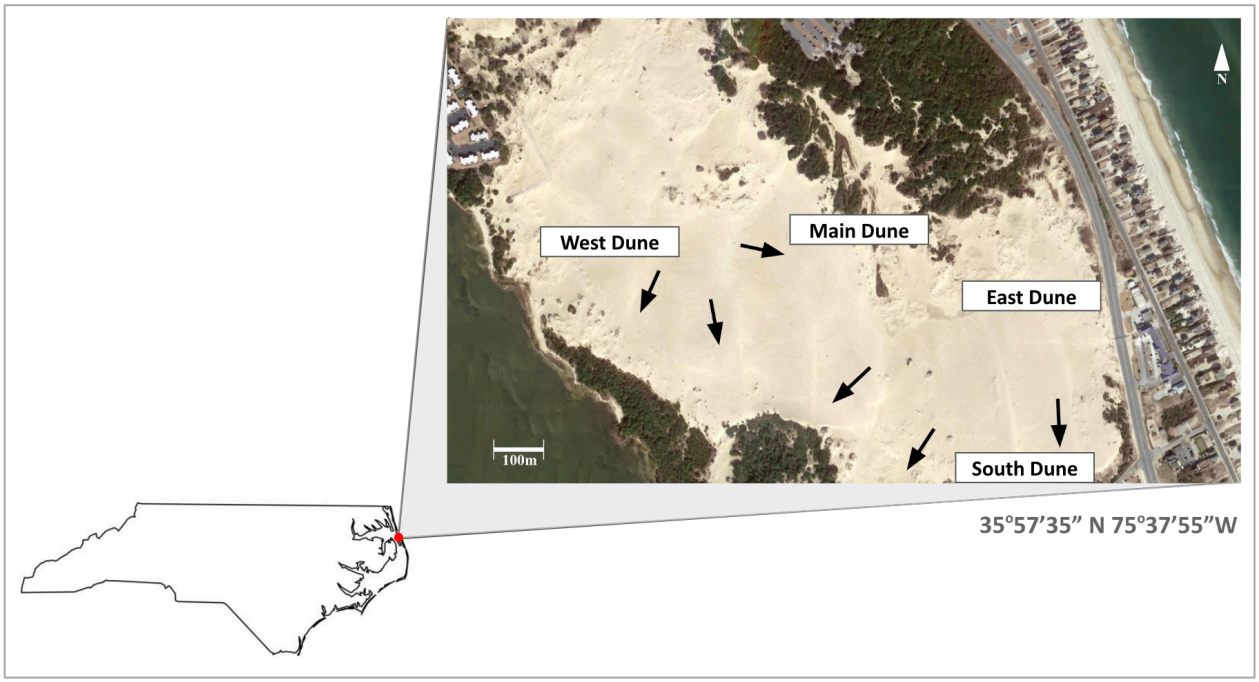

Figure 3. Jockey's Ridge State Park, NC. The four primary dunes are labeled with arrows depicting the general migration direction of each. The general migration of the entire dunefield is to the south. Image source: Google Earth/ TerraMetrics.

As the largest coastal dune complex in the eastern United States, Jockey's Ridge is simultaneously a vulnerable ecosystem and a popular recreation site (Mitas et al., 2014). Jockey's Ridge formed 3000 to 4000 years ago from strong hurricanes and currents depositing marine sand inland. Today, the park occupies 400 acres of land (Jefferys et al., 2019).

These factors, combined with the history of active dune migration, have made Jockey's Ridge a focus of dune research. For example, Mitasova et al. (2005) used time-series measurements of topography from high-resolution lidar to measure patterns of geomorphic change. They found that four main dunes comprise Jockey's Ridge; the largest of these dunes, called the "main dune", has been steadily decreasing in elevation since 1953, while the other secondary dunes have been increasing in elevation. All the dunes are migrating southward at a rate of 3 to 6 m/yr (Mitasova et al., 2005).

The migration direction has been consistent over the last several decades, indicating that non-wind factors such as park visitation, which has only occurred consistently at the park since 1975, have a negligible effect (Mitasova et al., 2005). The migration of the Jockey's Ridge dunefield creates a two-pronged problem: first, the dunes are moving out of official state park boundaries, meaning the state is losing managerial control over them; and second, sand threatens the infrastructure bordering the dunes, such as Soundside Road, an important access road to the park and nearby residential areas (Pelletier et al., 2009) (Figure 4).

Figure 4. Two perspectives of Soundside Road and the nearby infrastructure. An aerial view (left) shows the road marked in red and the dunefield to the north. A street view (right) shows the sand bypassing a fence and approaching the road. Image source: Google Earth / Airbus, 4/25/2023.

These impacts have motivated some interventions including fencing to intercept sand, and, as a last resort, manual relocation of sand using dump trucks (Pelletier et al., 2009). These efforts are extremely labor intensive: for example, in 2003, workers relocated approximately 125,000 m^3 of sand south dune and to the northern edge of the park (Pelletier et al., 2009). While both techniques have been somewhat effective in preventing sand from leaving the park, they also disturb the local ecosystem within an otherwise protected landscape. Questions on best management practices at the site continue to arise (Mitas et al., 2014). Therefore, a major goal is to improve predictions for dune migration to better inform their management.

1.3 Reduced complexity modeling

Numerical models for model dune formation and migration began to develop in the 1980s, initially focusing on detailed physics at the particle-scale interactions (Livingstone et al.,

2007). Werner (1995) proposed an alternative approach using a rules-based, reduced-complexity model (Paola & Leeder, 2011). He motivated this approach with two main arguments: first, dune fields evolve to a finite number of states from a broad range of initial conditions. Second, dune fields exhibit emergent behavior, meaning they self-organize on characteristic spatial and temporal scales (Kocurek & Ewing, 2005). Werner's model importantly generated dune-like morphologies without incorporating grain-scale processes that are computationally intensive to represent. Pelletier et al. (2009) expanded on Werner's model to account for the sediment-stabilizing effect of inter-dune vegetation, and applied to the model to interpret dune evolution at Jockey's Ridge.

1.4 Research question and hypothesis

While the Pelletier et al. (2009) model was successfully applied at Jockey's Ridge, it was implemented only for a unidirectional wind. In reality, the dunes at Jockey's Ridge instead experience bi-annual changes in overall wind direction; there is anecdotal evidence of the dunes shifting seasonally due to this wind pattern (Mitasova et al., 2005). From March to August, the most powerful winds are from the southwest; from September to February, the strongest winds originate from the northeast (Pelletier et al., 2009). The dunes experience a seasonal bimodal wind regime, where the wind travels in opposing directions for each half of the year (Bishop et al., 2001). Therefore, important knowledge gaps persist regarding how natural winds that vary in direction contribute to the long-term evolution of dunes at Jockey's Ridge, which impedes the development of effective strategies for land management.

This objective of this study is to test how **bimodal wind directions impact predictions for dune evolution using a reduced-complexity model.** I hypothesize that accounting for

variable wind directions will change model predictions in two ways. **First, I hypothesize that the predicted dune migration will create more ridge-like dunes than developed under the unidirectional winds in the Pelletier et al. (2009)** model. This behavior is expected since bimodal winds and high sand supply lead to the formation of ridges, not barchans (Figure 2). **Second, I hypothesize that the model with bimodal winds will predict slower southerly migration compared to the predictions that only account for winds in one direction.**

2 Previous model implementations

This section reviews some aspects of the implementation of the numerical models that provide a foundation for the analysis.

2.1 Werner (1995)

Werner developed his model to be more widely applicable than those with empirical constraints (e.g. Rubin, 1987). Instead of composing elevation from individual sand grains, Werner's model has initial conditions where sand particles are grouped into discrete, rectangular prism units— referred to as "slabs"— that are stacked across a lattice of cells (Figure 5).

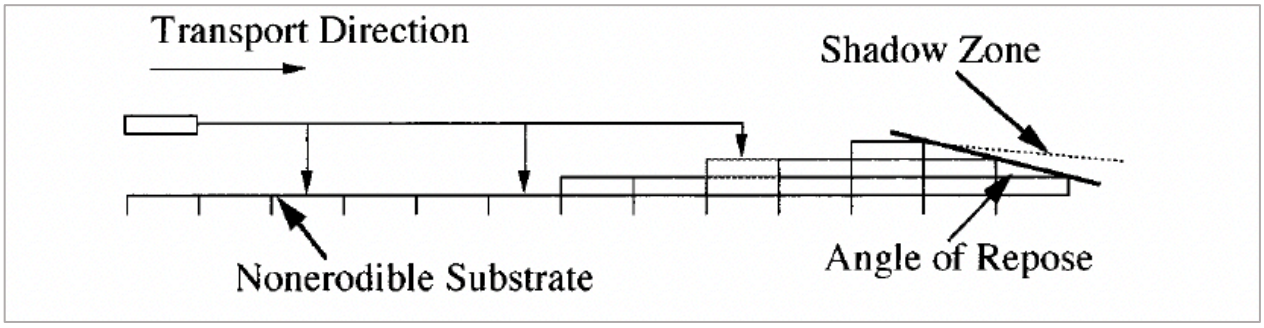

Figure 5. Diagram of the sand transport algorithm in Werner's model. Slabs are picked up, then moved in the transport/wind direction, then deposited as they move downwind. They accumulate to form a dune, shown on the right. This figure is adapted from (Werner, 1995), his Figure 1.

All slabs are set on top of a non-erodible surface akin to bedrock. Werner's main algorithm consists of 3 core rules that, when applied to a randomly generated elevation grid, lead to the formation of dunes. The rules are as follows:

(1) *Entrainment and deposit:* Slabs of sand are selected for entrainment at random. One slab at a time is considered for entrainment. The entrained slab is then transported a horizontal distance from its original position. The distance, known as "leap length" (l) is a proxy for wind strength, as it determines how far sand moves downwind. After the unit has traveled the set distance downwind, the probability of it being deposited depends on the contents of the depositing cell. The likelihood of deposition (p) is greater at a cell that contains sand than one that does not; this is due to the greater likelihood of rebound for grains on a smooth surface (Bagnold, 1997). The values of l and p define the qualities of sand flux in the modeled scenario (Pelletier et al., 2009).

(2) *Shadow zone:* A shadow zone is an area in shade parallel to the wind direction when the surface is illuminated by a sun angle of 15° (Pelletier et al., 2009) (Figures 1 and 6). Also known as the "wind shadow", it is the part of the dune that the wind cannot reach due to higher elevations blocking winds from reaching lower zones. The shadow zone is located on the lee side of the dune and is defined by minimal aeolian sand transport. In Werner's model, a slab in shadow is automatically deposited ($p = 1$).

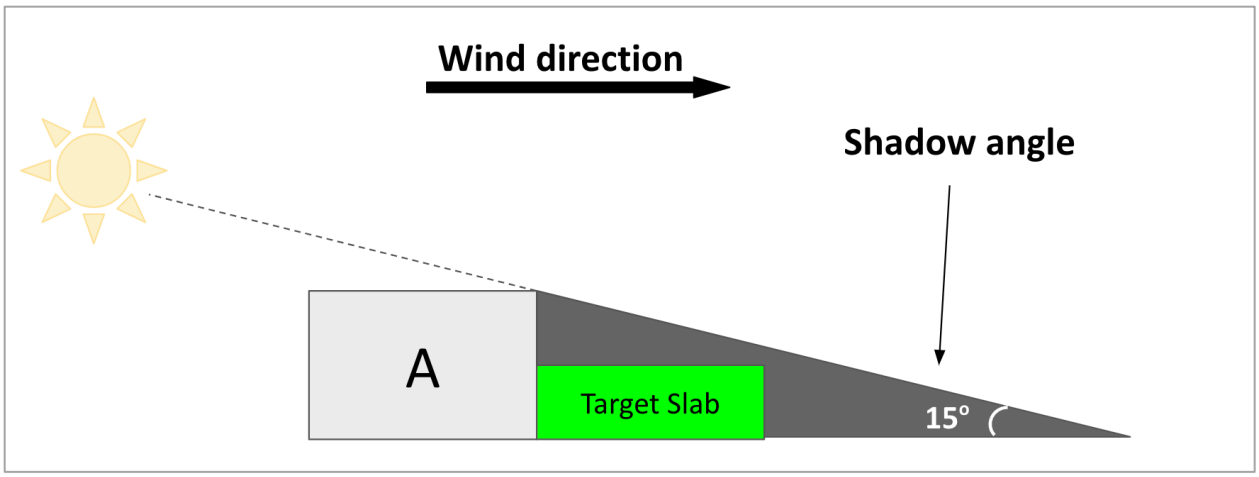

Figure 6. Diagram of the shadow zone. The target slab is in the wind shadow cast by slab A. Even though the sun is used to determine the location of the shadow zone, it plays no role in affecting deposition. Instead, using the sun angle as the convention to determine the extent of the shadow zone is more conducive to real-life dunes, since one can visualize where the wind cannot reach.

(3) *Avalanching:* Werner models the "avalanche effect" when the slope of the sand on the lee side of dunes is greater than the angle the dune makes with a horizontal surface, called the angle of repose (Sutton et al., 2013) (Figure 7). If the slope of the lee side of the dune is greater than the angle of repose, the slab will roll down at the angle of steepest descent (Livingstone et al., 2007). This effectively prevents the creation of divots and over-steepened peaks.

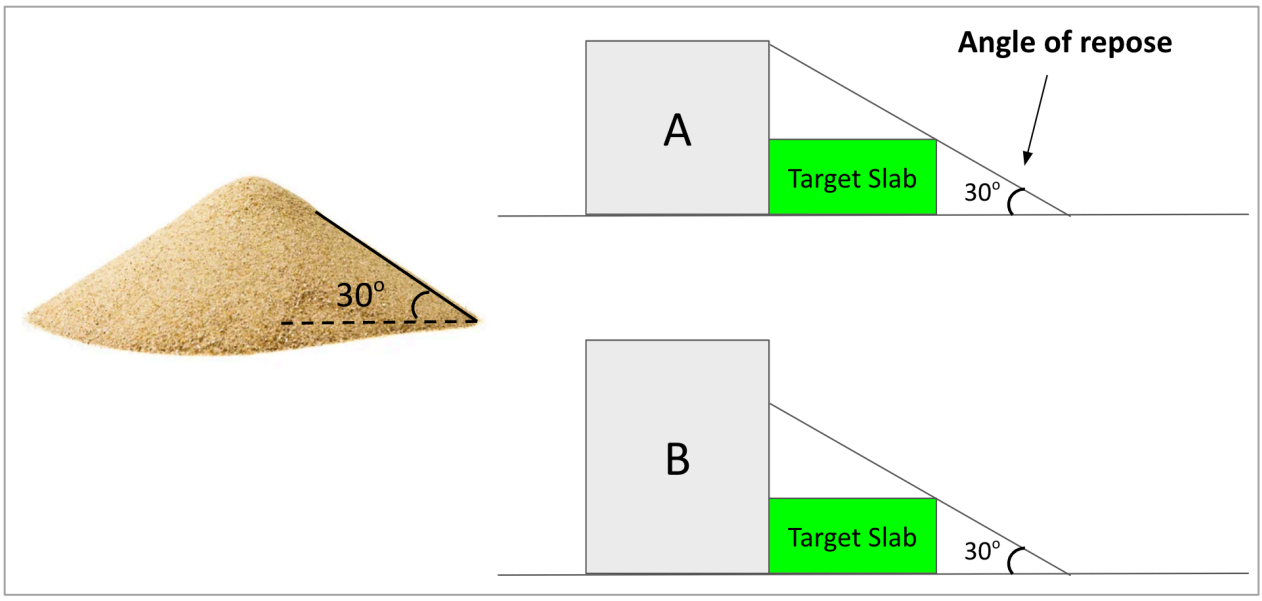

Figure 7. Angle of repose on a real sand pile and a diagram. The angle of repose is primarily based on the fiction of the specific grain comprising a pile; for medium-grain sand, it is 30°. Slab A does not exceed the angle of repose, so no avalanching would occur. Slab B creates an oversteepened slope, which would cause sand to transfer down the angle of steepest descent onto the target slab.

With these three components accounted for, Werner's model successfully forms a dune from an initial condition of randomly distributed slabs. Importantly, because the code from Werner (1995) was never published, later implementations were made based largely on the algorithm described in the original paper and therefore differ in detail.

2.2 Pelletier (2009)

Pelletier et al.'s (2009) study of Jockey's Ridge builds on the Werner (1995) model by adding a new factor: the probability of entrainment. This variable accounts for the fact that not all sand parcels have the same chance of undergoing transport. The main driver for this

variability is vegetation, which increases surface roughness and resists erosion (Pelletier et al., 2009). Several additional extensions are made to incorporate vegetation effects as follows:

(4) *Vegetation sand-trapping*: Vegetation in Jockey's Ridge only exists in significant amounts at low elevations. Sand at lower elevations is less likely to be moved due to the vegetation's sand-trapping properties. The lower the elevation, the less likely sand is to be entrained.

(5) *Oceanside shear* stress: Oceanside dune faces experience higher bed shear stress and thus have a higher probability of being entrained (Pelletier et al., 2009). In Jockey's Ridge, the ocean lies to the east; therefore, a cell's chance of entrainment decreases as it moves further west.

These two properties are combined in an equation for probability of entrainment as

$$p_e = (\frac{h}{h_{max}})^2(\frac{x}{x_{max}}) \quad (2)$$

where h_{max} is the maximum elevation of the dune, x is the distance from the west boundary, and x_{max} is the total horizontal distance across the dune field.

A further condition added is that slabs are not entrained if they are in wind shadow. While never explicitly stated in Werner's algorithm, most interpretations of his model implement this rule (Pelletier et al., 2009; Elder, n.d.). Importantly, the Pelletier et al. (2009) model is designed to work with dimensioned coordinates rather than grid cells, which simplifies its application to natural cases.

2.3 Other modifications to the Werner (1995) model

Other additions made to the Werner base model that are not accounted for in this research are briefly recounted here. These models are not suited for the goals of this research but should

be acknowledged in terms of the knowledge gaps they aim to address. Momiji and Warren incorporate variable sand-trapping efficiency, which results in dunes with longer windward than leeward faces (2000). This addition greatly increasing the number of model cycles required to form a dune, exceeding the limitations of reduced-complexity modeling (Momiji & Warren, 2000). Bishop et al. expands on Momji and Warren's model, testing it with Werner's parameters (2001). Specifically, they incorporate 8 cells for avalanching instead of 4, more accurately representing the real-life occurrence of diagonal adjacency (Bishop et al., 2001)

Further, like Pelletier (2009), Baas (2002) accounts for the effects of vegetation. However, instead of acknowledging vegetation's effect on entrainment, the Baas model assumes that the sand-trapping capacity of vegetation greatly reduces the lateral distance that a sand slab can travel. Since a cell undergoing a leap of distance l may be trapped when passing through a cell with vegetation, in this model sand jumps only one cell downwind at a time (Baas, 2002). These models still assume unilateral wind direction, so it is not possible to apply them to variable wind fields.

3 Methods

3.1 Model with wind variability

I used MATLAB to create the model for this study. Since this project demanded a thorough understanding of all model components and their interactions, as well as substantial extensions to enable variable wind directions, I developed a model from scratch. This approach offered precise control over each aspect, enabling deliberate adjustments for experimentation.

The model consists of a wrapper and a script. When a randomly generated elevation grid is put into the model, the output is a dunefield produced as a figure and/or a short video.

Inspiration for the base model was derived from Werner's written algorithm (1995), Pelletier et al.'s C++ code (2020), and other published interpretations in other coding languages (Goldstein, 2016; Elder, n.d.).

To set up the model, a square grid is created with a random elevation assigned to each cell. Each cell contains a stack of rectangular slabs of sand, which have a height equal to one-third of the width (Figure 8). The grid has periodic boundaries, meaning that if a slab is moved past the right-most boundary of the grid, it will return on the left.

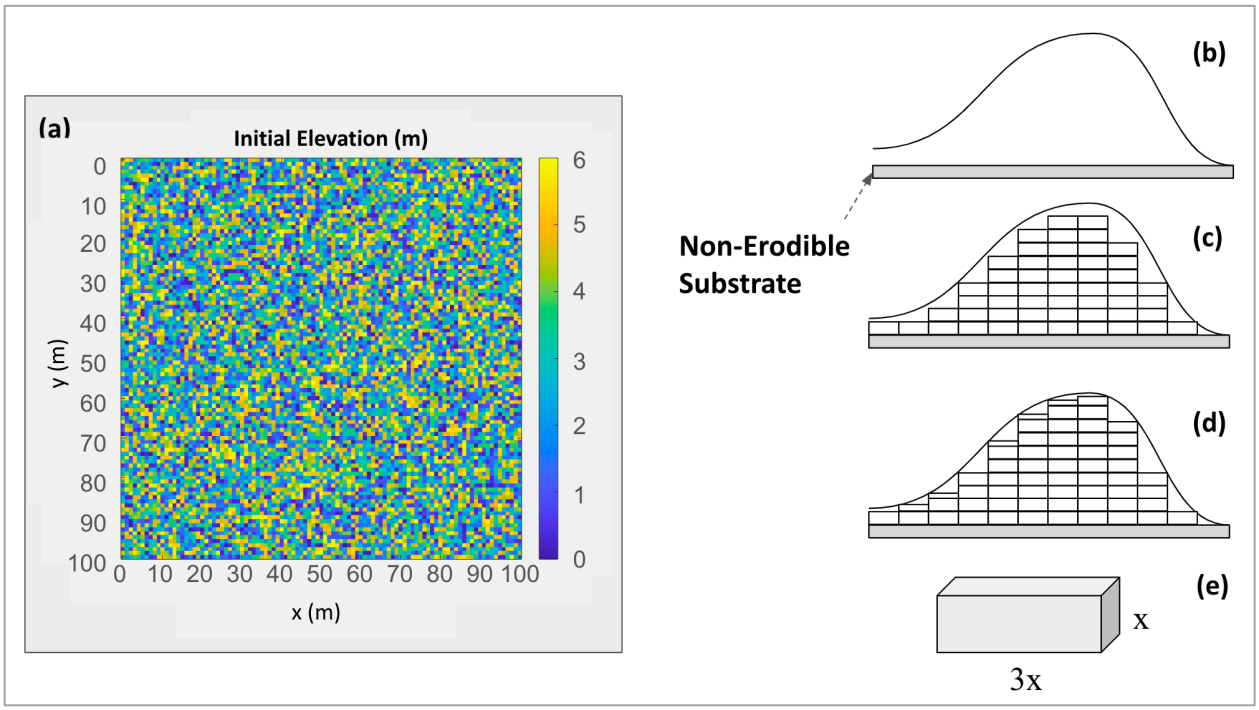

Figure 8. Base model set-up. Fig. 8a is a randomized 100 m x 100 m initial elevation grid. Figs. 8b-8d show a hypothetical horizontal plane view of a dune formed by slabs. 8b shows the general shape of a dune with a nonerodable surface forming a base. 8c shows the dune broken into slabs, and 8d shows the addition of partial slabs to best match the shape of the dune curve. 8e depicts a singular slab in 3D, including the 1:3 height to width ratio.

The model runs over a set number of time steps. Throughout each time step, every cell in the grid is polled for entrainment (Appendix A). Time in this model differs from nature. Instead of time relating to a set period (i.e. minutes or years), time relates to the number of instances in which every cell in the grid gets a chance at displacement (Elder, n.d.). For this model to reflect real timescales, p and l are used to relate sand flux to real-life sand flux speeds (Pelletier et al., 2009).

To start each individual iteration, a cell is selected at random from the entire grid. Before any sand is moved, the conditions of the cell are determined. First, the cell is checked for shadow. To do this, the angle between the elevation of the selected cell and the of the adjacent cells upwind of the cell is calculated (Figure 6). If this exceeds the shadow angle, then the cell is considered in wind shadow. For bimodal wind, the shadow conditions are checked in the component vectors of the slab transport (ex. for southwest wind, the selected cell is checked for shadows cast from the south and from the west) (Figure 9). To be considered "in shadow," a cell moving diagonally must have shadows cast on it from both directions. Second, the probability of entrainment is calculated for the selected cell using Equation 2.

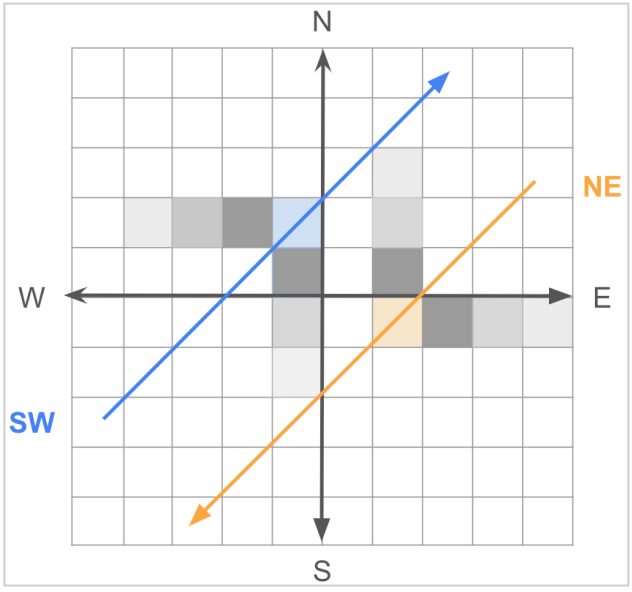

Figure 9. Shadowing conventions for diagonally-moving cells. Shadows are cast upwind in the directions of the components of the movement vector.

If the starting cell (a) contains no sand, (b) is in shadow, or (c) does not meet the probability threshold, it is ineligible for entrainment. In this case, no sand is moved, and a new cell is selected. New cells are selected until all three of the three entrainment conditions are false. Once it meets the conditions for entrainment, a slab of sand is removed from the initial cell. If there is less sand in the cell than the height of a whole slab, the amount of sand in the cell is entrained instead. Any necessary avalanching caused by the sand removal occurs, preventing divots from forming when the sand is moved (Figures 10 and 11).

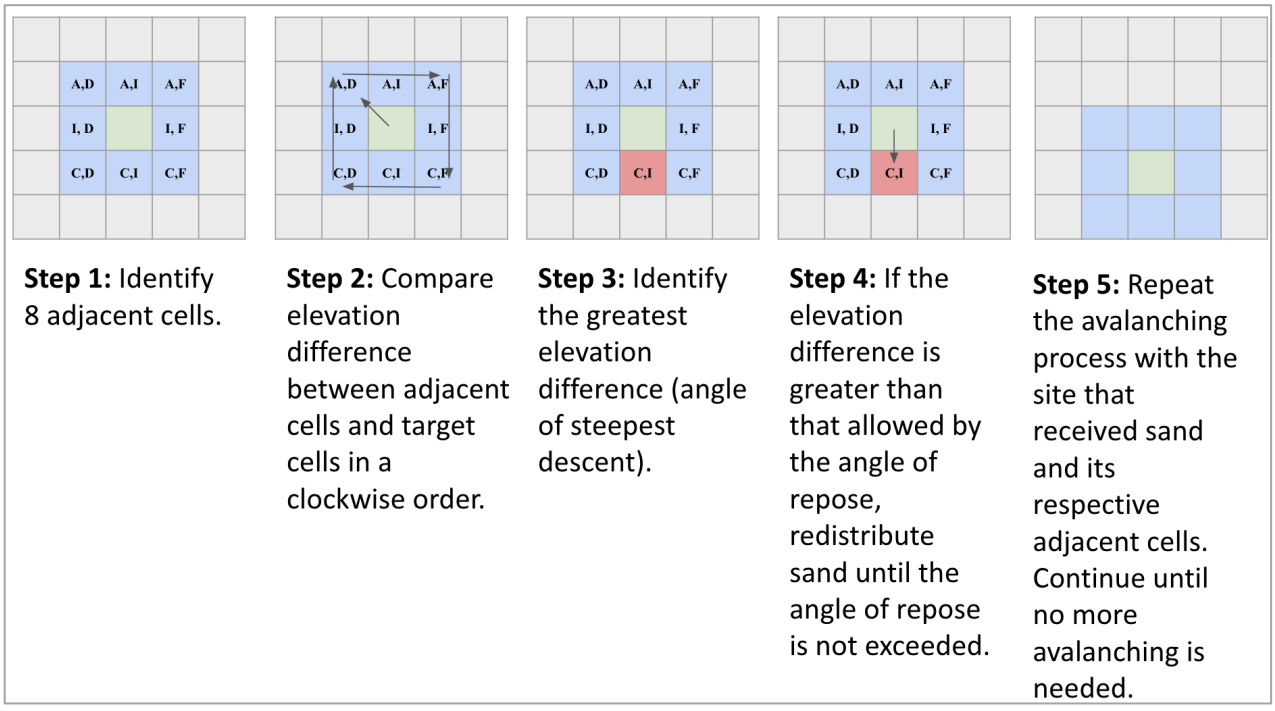

Figure 10. Algorithm for avalanching, which fills divots and flattens peaks. Avalanching is a recursive process, meaning that it can occur on any cells affected by the previous avalanche.

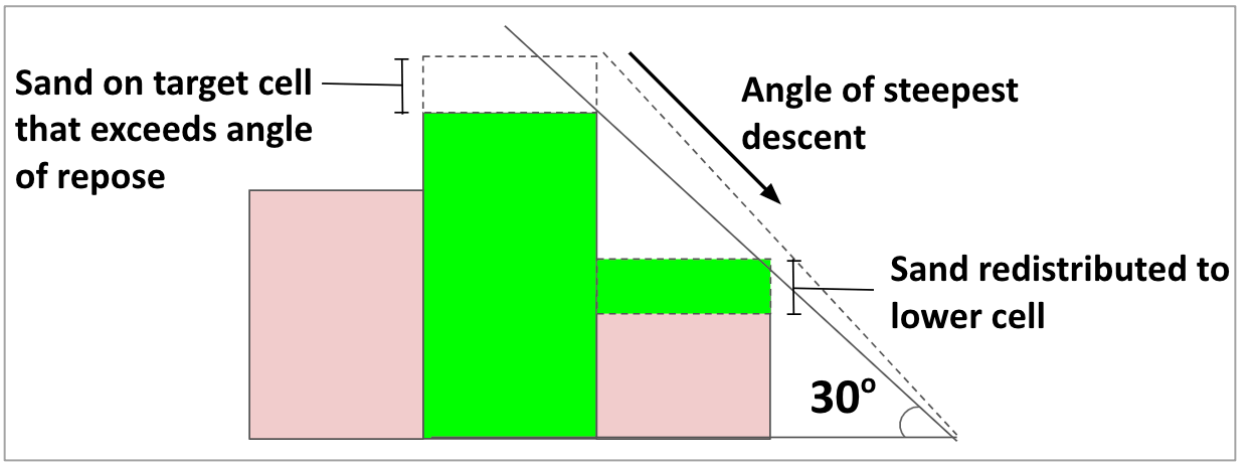

Figure 11. Horizontal view of elevation adjustments caused by sand redistribution during avalanching. The top the green cell is moved to the adjacent cell that forms the angle of steepest descent between elevations. It is moved so that the difference between the tallest cell and its adjacent counterpart do not exceed an elevation difference that causes an angle greater than 30°.

The slab is then moved downwind a distance (l) based on the wind strength. For bimodal wind conditions, the wind strength is set to different values for each direction. The slab is carried to a site called the "deposit cell." If the deposit cell is in shadow, then the slab is automatically deposited. If the deposit cell contains sand, the probability of deposition is set to 60%. If the deposit cell is empty, this chance decreases to 40%. A random probability value is generated. If this value is greater than the deposition probability, the sand is not deposited and is carried downwind again. This process is repeated until deposition occurs. During deposition, the height of the sand slab subtracted from the initial cell is added to the deposit cell. Avalanching is performed again to prevent any oversteepened peaks caused by the increase in elevation of the deposit cell (Figure 10).

This pattern is then repeated until all time steps have been completed. To account for seasonal switches in wind direction and speed, every time one time step is completed, the direction and value of l is switched.

With unilateral wind conditions, my model produces results consistent with those produced by the unilateral wind model from Werner (1995). Since the Werner's original model is not available, the best way to demonstrate consistency is through a visual comparison of model results (Figure 12). The creation of both barchans and barchanoid ridges from random initial elevations and low sand supply indicates a successful interpretation of Werner's principles.

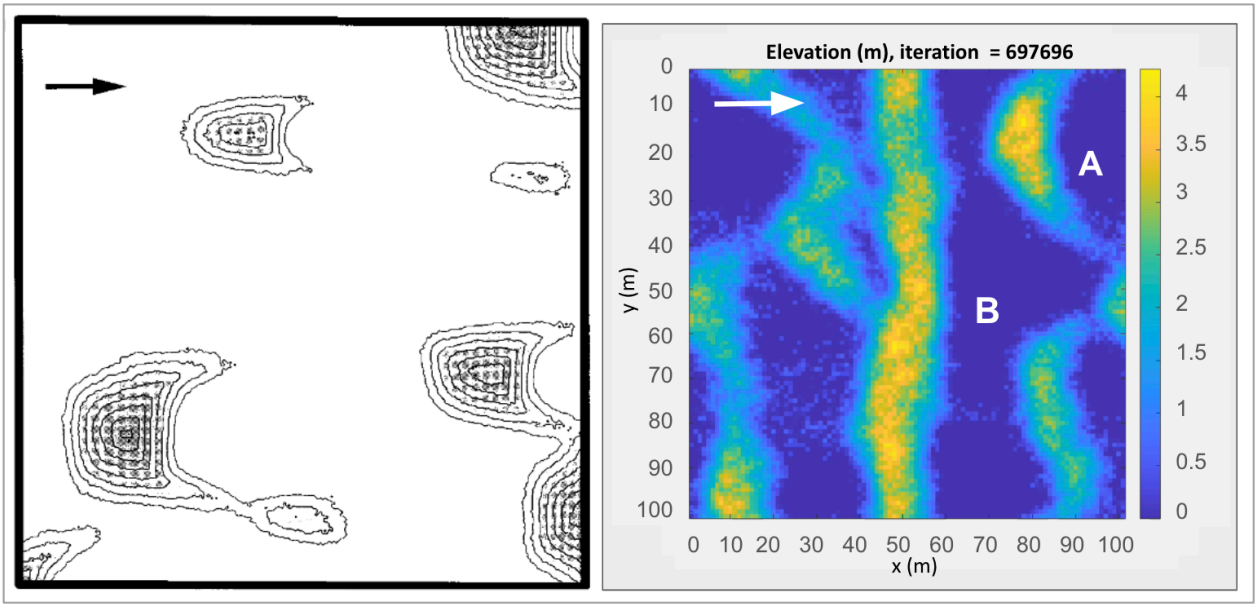

Figure 12. Comparison between Werner's 1995 model (left) and this paper's (right) base model. Both models used the same l, p_s, and p_{ns} values, and employ unidirectional eastern wind. Figure 13b reflects a barchan (A) that closely aligns with the structure of the dunes created in Werner's original model. Figure b also depicts a barchanoid ridge (B), which are formed with two or more adjacent barchans collide. This figure is adapted from (Werner, 1995), his Figure 2.

3.2 Novel model components

The base model can run with steady, unidirectional wind, or with wind that changes direction and strength. Unlike in previous models, a slab can move diagonally, changing both row and column. I introduce a new method of determining shadow conditions from multiple directions.

Since entrained slabs can now be moved out of the upper and lower boundaries of the model, the horizontal boundaries are now periodic. Further, unique l values are introduced for each wind direction. Depending on which wind direction is applied to a given cell, the distance l varies based on wind strength. To obtain the l values for the model applied to Jockey's Ridge, the average wind speeds from the NE and SW were divided to give a scalar factor. This scalar was applied to the distance l to account for the slightly stronger winds originating from the northeast. Finally, the wind direction changes each time the entire grid is polled for entrainment to represent wind seasonality.

3.3 Topography

In order to visualize the migration of dunes in Jockey's Ridge, the North Carolina State University OSGeo Research and Education Laboratory collected topographic imagery from 1999 to 2014 (Hardin et al., 2014). The topographic data was collected using NOAA's National Geodetic Survey Remote Sensing Division with an OPTECH ALTM system. Files containing data from 1999 and 2008 were loaded into MATLAB in .tif format, and real-life values were assigned to existing model variables. The DEMs were clipped to focus on the area of interest, which is the largest dune of Jockey's Ridge (commonly known as the "main dune" in related literature) (Figures 3 and 13).

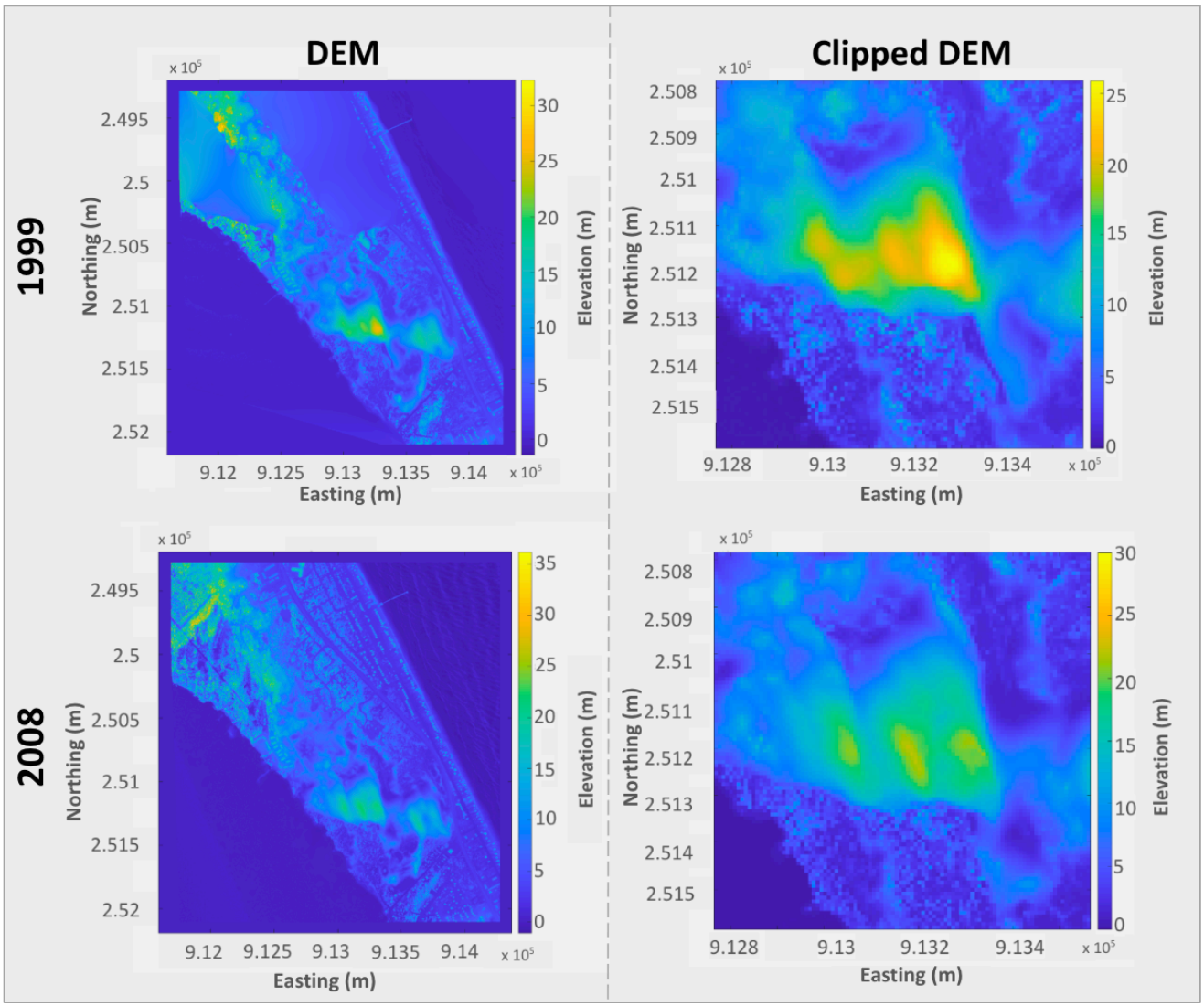

Figure 13. Digital elevation models for Jockey's Ridge with data collected in 1999 and 2008 by Hardin et al.

3.4 Future work

This work can be extended the model to add all four wind directions, as well as the ability to combine any of these four directions for bimodal winds. There is also room for experimentation with the Werner base model conditions to see if the logic behind his model can produce all the possible dune shapes based on wind variability and sand supply (Figure 2).

Finally, as instances of hurricanes increase due to climate change, the occurrences of large-scale wind events will also increase (Holland & Bruyère, 2014). Expanding the variable wind directions from the model to consider hurricanes as large stochastic events that greatly increase *l* could provide unique insight in upcoming research.

4 Model results and analysis

4.1 Run conditions

The effect of the additions to the base model were determined by running the following variations (Tables 1 and 2):

(a) Run 1: Unidirectional wind, randomly generated elevation

(b) Run 2: Unidirectional wind and variable entrainment, randomly generated elevation

(c) Run 3: Bimodal wind and variable entrainment, randomly generated elevation

(d) Run 4: Unidirectional wind, 1999 Jockey's ridge DEM

(e) Run 5: Unidirectional wind and variable entrainment, 1999 Jockey's ridge DEM

(f) Run 6: Bimodal wind and variable entrainment, 1999 Jockey's Ridge DEM

	Parameters in Code					
Model run	Wind direction	*l*	Variable entrainment	Maximum dune height (m)	Distance to West boundary (m)	Initial topography type
1	south	5	false	-	-	random
2	south	5	true	3	100	random
3	bimodal	5.3 (NE), 5 (SW)	true	3	100	random
4	south	5	false	-	-	DEM
5	south	5	true	30	1200	DEM
6	bimodal	5.3 (NE), 5 (SW)	true	30	1200	DEM

Table 1. Parameter values for each model run.

Parameter	Value	Parameter	Value
Grid spacing	1 m	p_ns	0.4
x_max, y_max	100 m	p_s	0.6
Maximum Initial z	2/3 m	Angle shadow	15º
Baseline depth	0 m	Angle repose	30º
Slab height nominal	1/3 m	Time max	100

Table 2. Parameter values that were consistent across all model runs.

4.2 Random elevation outcomes

The model produced elevations for $t = 0$, $t = 50$, and $t = 100$ for each of the three model conditions (Figure 14). Over time, the unidirectional wind model with equal entrainment probabilities (run 1) self-organized into barchans, barchanoid ridges, then a single ridge. The accumulated height of the ridge is over 3 times the maximum starting height for a cell. The unidirectional wind model with varying entrainment (run 2) demonstrated an elevation gradient driven by entrainment in early iterations, as demonstrated by higher elevations accumulating closer to the west boundary. The final state of the model indicates the very beginnings of horizontal ridge formation, but no clear dunes arose within the timeframe. The elevation grid flattened over time, with the maximum height decreasing from 2 m to 1.8 m. The bimodal wind model (run 3) showed an extreme elevation gradient after only 10 iterations. Sand moves from the northeast and wraps vertically, causing sand slabs to accumulate towards the west boundary, forming a structure similar to a transverse dune. The gradient steepens over time, and the maximum height of the ridge is approximately 1.75x higher than the original random elevation grid.

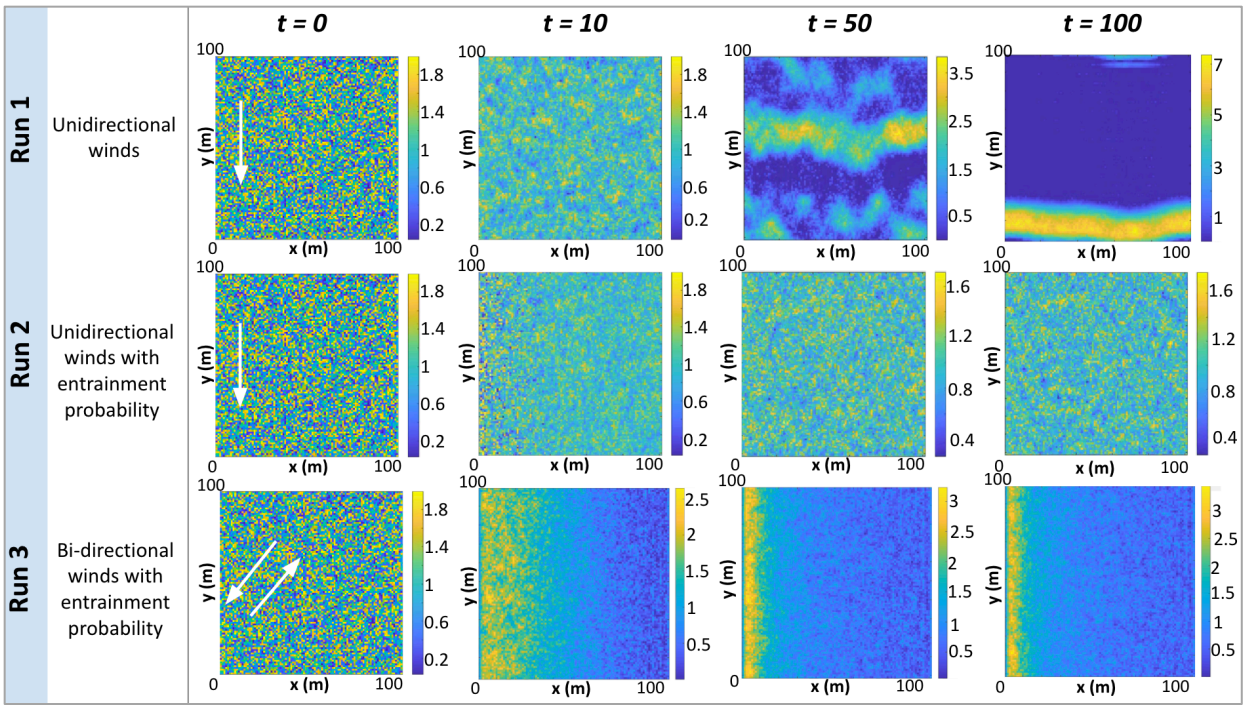

Figure 14. Results for runs 1-3 from application to a random elevation grid with a starting maximum elevation of 2. *t* is the number of times that the entire grid is polled for cell movement. Elevation is in meters. Note that the scales of elevation bars vary. The arrows represent the wind direction(s) for each model run. In Run 1, with unidirectional southern wind and an equal chance of entrainment, barchans and barchanoid ridges formed. In Run 2, with unidirectional southern wind and varying chance of entrainment for all cells, the overall elevation decreased. In Run 3, with bimodal northeast/southwest wind and varying chance of entrainment, a distinct ridge was formed on the inland boundary.

The models with unidirectional wind behaved as expected. Barchans formed in the base model, aligning with Werner's own outcomes from his original model (1995) (Figure 14). Pelletier et al. do not share any results of their model applied to a random grid to compare to visually, but the outcomes above align with their written logic (2009). The flattening of the

overall elevation is due to the stabilizing effect of vegetation which limits entrainment of lower sand (Nield & Baas, 2008; Durán & Moore, 2013).

Since it contains entrainment probability conditions that rely on real-life values (maximum dune height and distance to ocean; see Equation 2), which are not as conducive to random-elevation based modeling in terms of self-organizing dune structures, the bimodal wind model was not expected to produce realistic topography on a random setting. Rather, the exhibited behavior of the bimodal wind model proxies how slabs will move when the algorithm is applied to real topography. As the model progresses, the northeastern-originating winds overpower the southwestern winds, driving slabs in the southwest direction. Unlike run 2, run 3 increased peak height, showing overall accumulation despite the flattening effect of vegetation sand-trapping.

4.3 DEM elevation outcomes

Runs 4-6 produced transformations of the clipped Jockey's Ridge DEM for $t = 10$, $t = 25$, and $t = 50$ (Figure 15). The main dune has three peaks, with the tallest on the right. The unidirectional wind model showed slight southern migration and increased elevation of the two smaller peaks in the dune. Barchan-shaped curves become more pronounced in both the peaks and trenches. When entrainment probability was added, a further southern migration occurred, and the dune flattened. The addition of bimodal winds showed a less significant flattening of the dune, and southwestern migration.

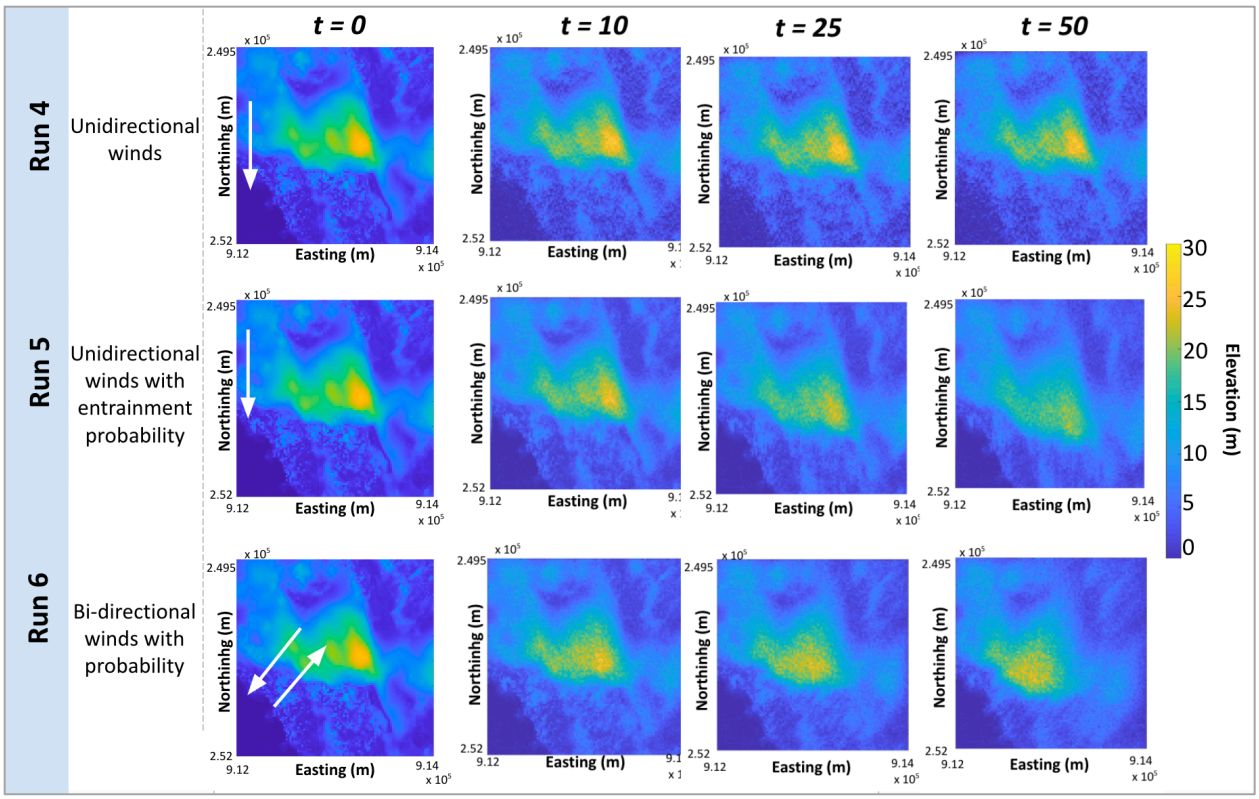

Figure 15. Results for runs 4-6 from application to 1999 DEM of the main dune from Jockey's Ridge. *t* is the number of times that the entire grid is polled for cell movement. Note that the scales of elevation stay constant in all subfigures. The arrows represent wind direction for each model class. In run 4, with unidirectional southern wind and an equal chance of entrainment, barchanoid angles formed and the peak migrated south. In run 5, with unidirectional southern wind and varying chance of entrainment for all cells, peak elevation decreased and southern migration occurred. In run 6, with bimodal northeast/southwest wind and varying chance of entrainment, overall elevation decreased and the peak migrated to the southwest.

The migration of the unidirectional wind model is similar to that published by Pelletier (Figure 16). Both show the main dune's peak forming a "W"-shaped barchan, and the beginnings of the formation of the signature barchan "horns". A visual comparison to Pelletier's results from their own unidirectional wind model shows that the interpretation of their vegetation-trapping

algorithm in this paper was fairly accurate (Figure 17). Pelletier applied their model to a 1974 DEM, so the dune structure is different; however, the consistent flattening of all dune peaks reflect the known effect of vegetation at Jockey's Ridge (Durán & Moore, 2013).

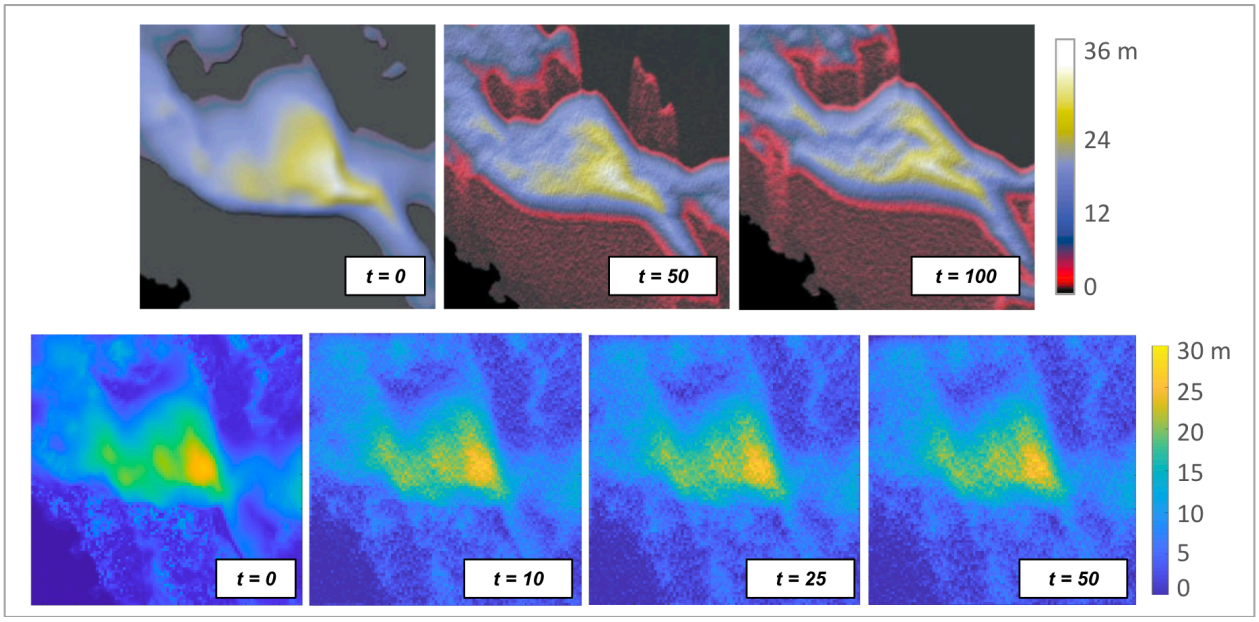

Figure 16. A comparison between two models of unidirectional wind applied to a Jockey's Ridge DEM (Pelletier et al., 2009). The upper DEM's initial elevation is from 1974, and the lower DEM's initial elevation is from 1999. The main dune is demarcated with a white peak in the Pelletier images. Both demonstrate southern migration and the increase of barchan patterns. Upper figures adapted from (Pelletier et al., 2009) their Figure 4.

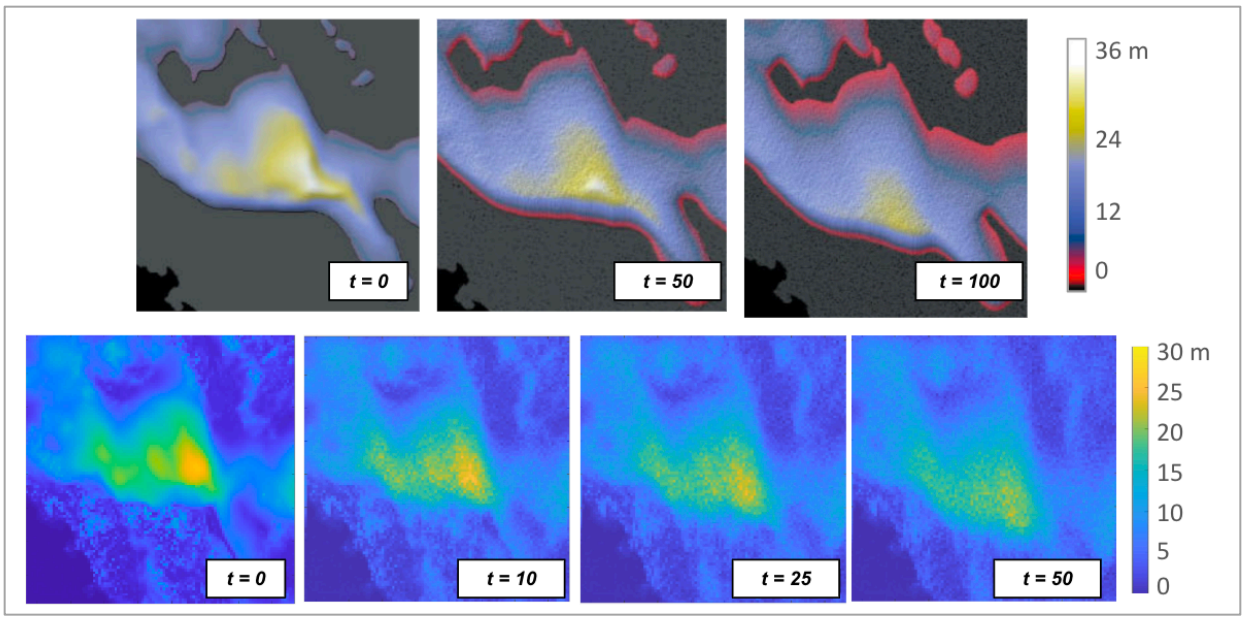

Figure 17. A comparison between two models of unidirectional wind with entrainment probability applied to a Jockey's Ridge DEM (Pelletier et al., 2009). The upper DEM's initial elevation is from 1974, and the lower DEM's initial elevation is from 1999. The main dune is demarcated with a white peak in the Pelletier images. Both figures depict a southern migration of the dune peak and overall flattening of the dune. Upper figures adapted from (Pelletier et al., 2009) their Figure 5.

5 Discussion

5.1 Random elevation model: Longitudinal dunes

As shown by the visual time series comparisons, there is a distinct difference in both individual slab movement and dune migration in the bimodal wind model. The sand accumulation is not barchan-shaped when the opposing winds are implemented into the random-elevation model. Instead, it more closely resembled the structure of linear dunes. Linear dunes are characterized by moderately variable wind conditions and low wind supply (Figure 2). Unlike transverse dunes, linear dunes migrate parallel to wind direction. Winds from opposite

directions that strike the dune obliquely are responsible for sand transport and erosion in linear dunes (Tsoar, 1983). These dynamics, combined with the lower entrainment on the west side of the model field, account for the formation of the vertical ridge.

However, as previously noted, caution must be exercised when analyzing the bimodal wind model applied to the randomized elevation. Instead of being expected to produce realistic dunes, the model's value lies in demonstrating how individual slabs will move. Slabs moved generally to the southwest, which is explained by the overpowering of the winds originating from the southwest by those from the northeast. In Jockey's Ridge, the prevailing southwest winds from March through August range from 9.9–12.8 mph while those from northeast in September through February range from 10.8–13.4 mph (Pelletier et al., 2009). Since the wind flux in the model was scaled appropriately to reflect the ratio between the seasonal wind strengths, the eventual migration to the southwest is explained by the greater wind strength, which is employed in the model as a proportionally longer leap length.

5.2 Digital elevation model: Differences in migration

The crux of the second hypothesis lies in the differences in projected dune migration of the unidirectional wind model and the bimodal wind model. Despite both starting and ending with the same cumulative elevation, the relative displacement of sand by each model varied greatly (Figure 18). Generally, the bimodal wind model predicted more sand further to the west, while the unidirectional wind model generated more sand to the east.

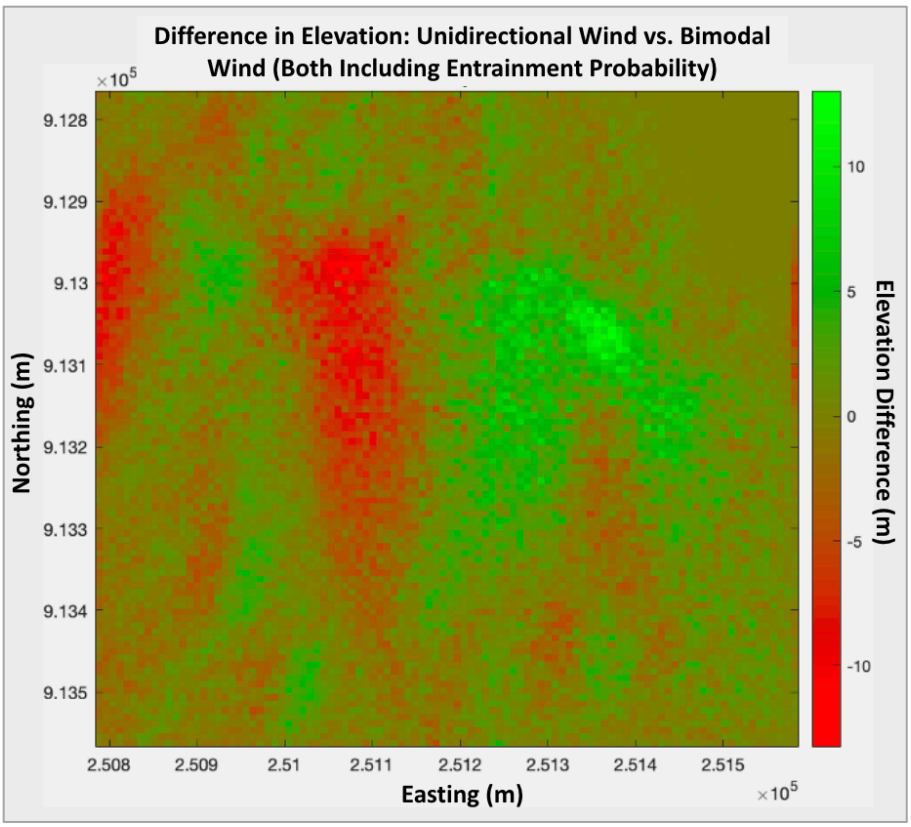

Figure 18. An elevation difference map between the DEM entrainment probability model runs with and without bimodal wind. The unimodal wind DEM was subtracted from the bimodal DEM to calculate the elevation difference at each cell. Green regions indicate areas where the bimodal wind DEM was higher, and red regions indicate areas where the unimodal wind DEM was higher.

While neither model was calibrated to actual time scales, comparing them to the 2008 DEM can provide useful insight into the differences in model behavior. In 2008, the furthest southern point of the dune body is UTM Northing 251,249. The approximate relative migration speed of each model can be estimated by determining the iteration at which each lee edge projects the dune at this point. It took longer for the experimental model to migrate to the 2008 southern dune boundary, indicating that southern migration occurred at a slower pace (Figure 19).

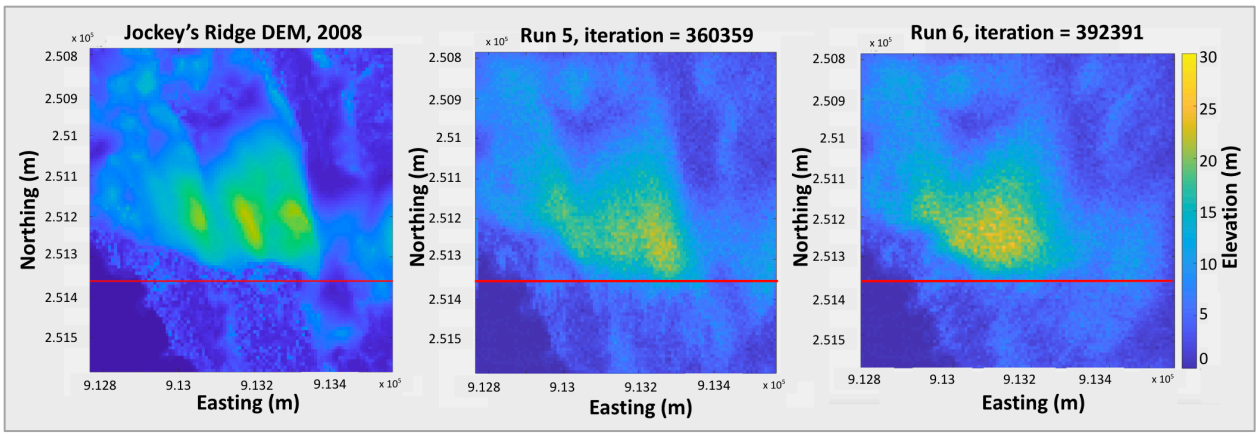

Figure 19. Southern boundary of main dune body in 2008 JR DEM (left), run 5 (center), and run 6 (right). The red line represents a latitude at UTM Northing 251,249. Elevation is in meters. Run 6, which had bimodal winds, took more iterations before migrating to the known 2008 location, indicating that it is a relatively slower migration that of run 5, which had only unimodal wind.

Another primary difference in the migration models is the fact that the three sub-peaks on the main dune merged into one peak in the experimental model. This merging is a result of the opposing winds, which drove the dune peaks together. Further, the bimodal wind dune did not flatten as much as it did with unimodal conditions. This transformation is likely due to the southwestern movement of sand in the experimental model overrode the lower rates of entrainment on the western parts of the dune (Parteli et al., 2009).

6 Conclusions

I built a reduced-complexity model to predict changes in dune formation and migration when bimodal wind conditions are incorporated. I also incorporated the effect of vegetation and oceanside shear stress on sand entrainment, inspired by an earlier application to Jockey's Ridge

by Pelletier et al. (2009). I applied this model to a random elevation grid and to DEM of the main dune in Jockey's Ridge State Park.

When compared to models applied to random elevations with unimodal wind conditions, the bimodal wind produced a distinct ridge and depicted sand slabs moving to the southwest. This behavior supports the hypothesis that bimodal winds cause ridges instead of barchans and supports earlier work on the relationship between sand supply and wind variability. Hindcasts run on a 1999 DEM of Jockey's ridge show distinct differences in sand movement with and without bimodal winds. With unidirectional winds, migration is directly south. When a probability of entrainment is added, this migration is coupled with an overall deflation of the dune. Bimodal winds cause the dune to migrate in the southwest direction and maintain a high peak. These outcomes, when compared to a DEM from 2008, demonstrate that while the unimodal wind model more accurately represents the southern migration of the dune, the bimodal wind model more accurately maintains the dune's peak elevation. This behavior is likely due to the impact of opposing forces on slabs that have lower chances of entrainment. Comparisons to the 2008 DEM also show that only accounting for unimodal winds causes faster predicted migration than bimodal winds.

This work suggests that predictions for dune evolution at Jockey's Ridge can likely be improved by accounting for the effects of variable wind directions. Future work can advance this goal by calibrating the model to use real-world timescales for sediment flux as grounded in timeseries topography observations.

References

Baas, A. C. W. (2002). Chaos, fractals and self-organization in coastal geomorphology: Simulating dune landscapes in vegetated environments. *Geomorphology*, *48*(1), 309–328. https://doi.org/10.1016/S0169-555X(02)00187-3

Bagnold, R. A. (1997). The nature of saltation and of 'bed-load' transport in water. *Proceedings of the Royal Society of London. A. Mathematical and Physical Sciences*, *332*(1591), 473–504. https://doi.org/10.1098/rspa.1973.0038

Bishop, S. R., Momiji, H., Carretero-González, R., & Warren, A. (2001). Modelling desert dune fields based on discrete dynamics. *Discrete Dynamics in Nature and Society*, *7*, 7–17. https://doi.org/10.1080/10260220290013462

Durán, O., & Moore, L. J. (2013). Vegetation controls on the maximum size of coastal dunes. *Proceedings of the National Academy of Sciences*, *110*(43), 17217–17222. https://doi.org/10.1073/pnas.1307580110

Gadal, C., Delorme, P., Narteau, C., Wiggs, G. F. S., Baddock, M., Nield, J. M., & Claudin, P. (2022). Local wind regime induced by giant linear dunes: Comparison of era5-land reanalysis with surface measurements. *Boundary-Layer Meteorology*, *185*, 309–332. https://doi.org/10.1007/s10546-022-00733-6

Goldstein, E. (2016, October 28). *Werner 1995 Cellular Dune Model*. GitHub. https://github.com/ebgoldstein/wDune95/blob/master/Werner95.py

Hardin, E., Mitasova, H., Tateosian, L., & Overton, M. (2014). *GIS-based Analysis of Coastal Lidar Time-Series*. Springer New York. https://doi.org/10.1007/978-1-4939-1835-5

Hersen, P. (2004). On the crescentic shape of barchan dunes. *The European Physical Journal B - Condensed Matter and Complex Systems*, *37*(4), 507–514. https://doi.org/10.1140/epjb/e2004-00087-y

Holland, G., & Bruyère, C. L. (2014). Recent intense hurricane response to global climate change. *Climate Dynamics*, *42*(3), 617–627. https://doi.org/10.1007/s00382-013-1713-0

Jefferys, K. M., Gray, P. C., Adams, C., Ridge, J. T., & Johnston, D. W. (2019). Monitoring change in sand dunes and swamp forests with google earth engine: Decadal ecosystem variability in an ecological preserve. *American Geophysical Union, Fall Meeting 2019*. AGU Fall Meeting Abstracts. https://ui.adsabs.harvard.edu/abs/2019AGUFM.B11I2299J

Kocurek, G., & Ewing, R. C. (2005). Aeolian dune field self-organization – implications for the formation of simple versus complex dune-field patterns. *Geomorphology*, *72*(1), 94–105. https://doi.org/10.1016/j.geomorph.2005.05.005

Livingstone, I., Wiggs, G. F. S., & Weaver, C. M. (2007). Geomorphology of desert sand dunes: A review of recent progress. *Earth-Science Reviews*, *80*(3), 239–257. https://doi.org/10.1016/j.earscirev.2006.09.004

Marín, L., Forman, S. L., Valdez, A., & Bunch, F. (2005). Twentieth century dune migration at the Great Sand Dunes National Park and Preserve, Colorado, relation to drought variability. *Geomorphology*, *70*(1), 163–183. https://doi.org/10.1016/j.geomorph.2005.04.014

McKee, E. (1979). *A study of global sand seas* (Vol. 1052). US Government Printing Office.

Mitas, O., Mitasova, H., Brothers, G., & Weaver, K. (2014). Managing dune landscape changes at jockey's ridge state park, north carolina. *Tourism in Marine Environments*, *9*(3–4), 155–167. https://doi.org/10.3727/154427313X13818453739477

Mitasova, H., Overton, M., & Harmon, R. S. (2005). Geospatial analysis of a coastal sand dune field evolution: Jockey's Ridge, North Carolina. *Geomorphology*, *72*(1), 204–221. https://doi.org/10.1016/j.geomorph.2005.06.001

Momiji, H., & Warren, A. (2000). Relations of sand trapping efficiency and migration speed of transverse dunes to wind velocity. *Earth Surface Processes and Landforms*, *25*(10), 1069–1084. https://doi.org/10.1002/1096-9837(200009)25:10<1069::AID-ESP117>3.0.CO;2-D

Paola, C., & Leeder, M. (2011). Simplicity versus complexity. *Nature*, *469*(7328), 38–39. https://doi.org/10.1038/469038a

Paris, A., Peytavie, A., Guérin, E., Argudo, O., & Galin, E. (2019). Desertscape Simulation. *Computer Graphics Forum*, *38*. https://doi.org/10.1111/cgf.13815

Parteli, E. J. R., Durán, O., Tsoar, H., Schwämmle, V., & Herrmann, H. J. (2009). Dune formation under bimodal winds. *Proceedings of the National Academy of Sciences*, *106*(52), 22085–22089. https://doi.org/10.1073/pnas.0808646106

Pelletier, J. D. (2020, September 17). *Model: Eolian dune model*. CSDMS. https://csdms.colorado.edu/wiki/Model:Eolian_Dune_Model

Pelletier, J. D., Mitasova, H., Harmon, R. S., & Overton, M. (2009). The effects of interdune vegetation changes on eolian dune field evolution: A numerical-modeling case study at Jockey's Ridge, North Carolina, USA. *Earth Surface Processes and Landforms*, *34*(9), 1245–1254. https://doi.org/10.1002/esp.1809

Rubin, D. M. (1987). Cross-bedding, bedforms and paleocurrents: Tulsa, Oklahoma. *Society of Economic Paleontologists and Mineralogists*.

Sutton, S. L. F., Neuman, C. M., & Nickling, W. (2013). Avalanche grainflow on a simulated aeolian dune. *JGR Earth Surface*, *118*(3), 1767–1776. https://doi.org/10.1002/jgrf.20131.

Swanson, T., Mohrig, D., Kocurek, G., & Liang, M. (2017). A Surface Model for Aeolian Dune Topography. *Mathematical Geosciences*, *49*(5), 635–655. https://doi.org/10.1007/s11004-016-9654-x

Tsoar, H. (1983). Dynamic processes acting on a longitudinal (seif) sand dune. *Sedimentology*, *30*(4), 567–578. https://doi.org/10.1111/j.1365-3091.1983.tb00694.x

Tsoar, H. (2005). Sand dunes mobility and stability in relation to climate. *Physica A: Statistical Mechanics and Its Applications*, *357*(1), 50–56. https://doi.org/10.1016/j.physa.2005.05.067

Tsoar, H., Blumberg, D. G., & Stoler, Y. (2004). Elongation and migration of sand dunes. *Geomorphology*, *57*(3–4), 293–302. https://doi.org/10.1016/S0169-555X(03)00161-2

Werner, B. T. (1995). Eolian dunes: Computer simulations and attractor interpretation. *Geology*, *23*(12), 1107–1110. https://doi.org/10.1130/0091-7613(1995)023<1107:EDCSAA>2.3.CO;2

Appendix A: Flowchart of model algorithm

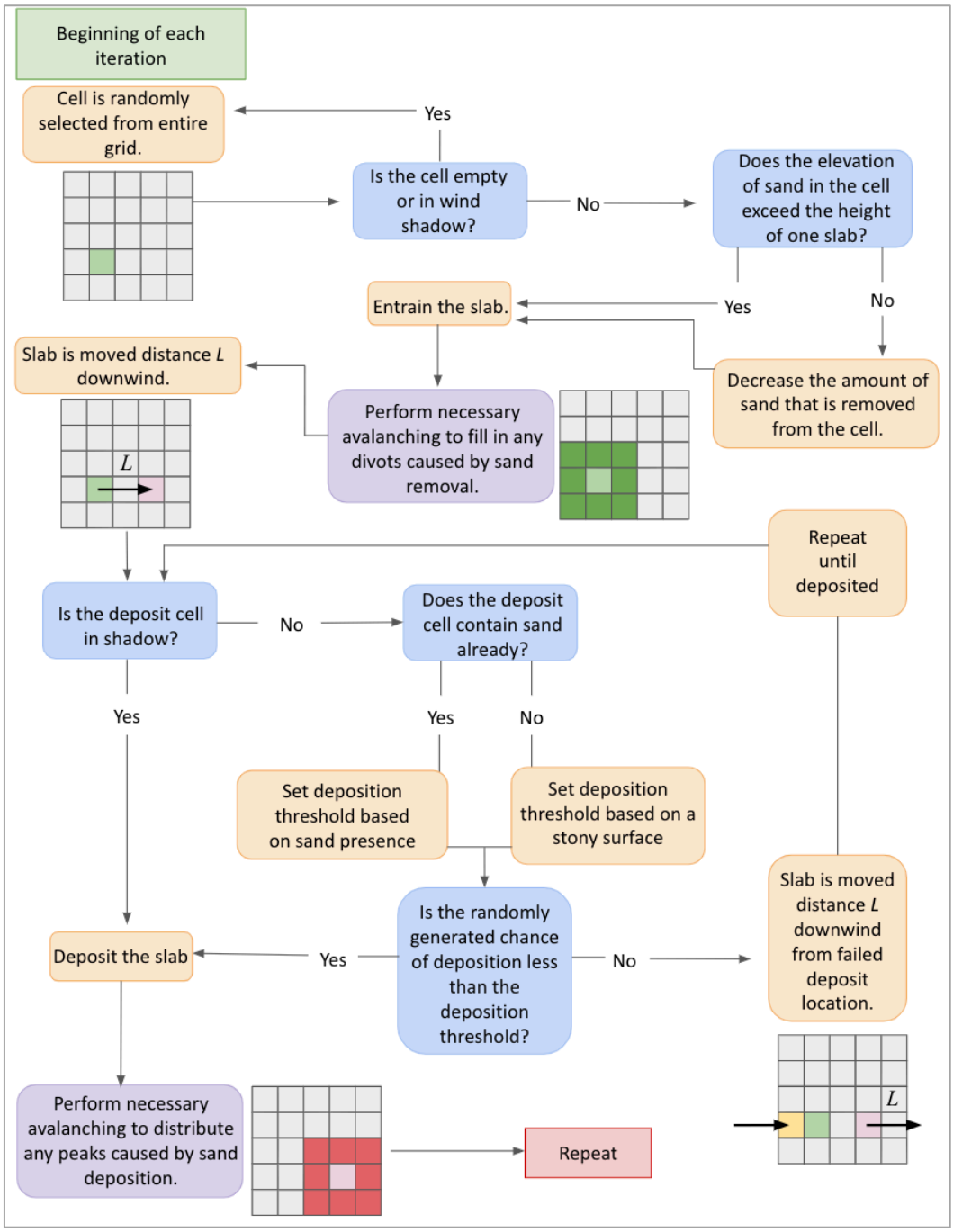

Figure A. Flowchart depiction of the main loop algorithm. Orange rectangles are steps, blue rectangles are conditional elements, and purple elements are functions that move sand aside from the main function (i.e., avalanching).